Evaluating Unicast and MBSFN in Public Safety Networks

Chunmei Liu*, Chen Shen*, Jack Chuang*, Richard A. Rouil*, and Hyeong-Ah Choi†
*Wireless Networks Division, National Institute of Standards and Technology, USA
†Department of Computer Science, George Washington University, USA
Email: *{chunmei.liu, chen.shen, jack.chaung, richard.rouil}@nist.gov, †{hchoi}@gwu.edu

***Abstract*—Public safety incidents typically involve significant amount of group traffic and have a stringent requirement on connection reliability. Hence multicast could potentially improve network and user performance significantly. Towards this goal, in this paper we investigate Long-Term Evolution (LTE) Multicast Broadcast Single Frequency Network (MBSFN) from the perspectives of throughput, resource efficiency, sources of MBSFN gain, and outage. Firstly, we derive a realistic MBSFN Signal-to-Interference-plus-Noise Ratio (SINR) analytical model, with multiple antennas, multipath channel, and equalizer considered. Secondly, we develop an MBSFN system level simulator as well as a simulation platform to compare unicast and MBSFN performance. Thirdly, we perform comprehensive simulations on the metrics under study. Through simulations, we discover that while unicast may achieve higher information bits/symbol, MBSFN provides higher throughput, and MBSFN throughput increases with MBSFN area size. We then quantify the MBSFN SINR improvement due to diversity combining and interference reduction, respectively. Furthermore, we show that compared with unicast, MBSFN improves outage probability significantly, which is essential for public safety incidents. Finally, we show that all the above MBSFN performance improvements apply to different MBSFN area sizes, even when the MBSFN size is one cell.**

***Index Terms*—Public safety, LTE, MBSFN, SINR analytical model, outage probability, resource efficiency.**

I. Introduction

Public safety mission is essential to protect citizens' lives and properties, and effective communications among first responders during public safety incidents is crucial. Compared with commercial traffic, public safety incidents typically involve significant amount of group traffic among first responders [1], including traffic intensive applications, such as mission critical video. Using traditional point-to-point unicast transmission at physical (PHY) layer to serve this type of traffic would require significant amount of spectrum, and sometimes lead to severe network congestion. With the above in mind, using multicast to serve public safety traffic has been put on the table, and Multicast Broadcast Single Frequency Network (MBSFN) in Long-Term Evolution (LTE) is one candidate due to its multicast nature and potential Signal-to-Interference-plus-Noise Ratio (SINR) improvement especially at cell edges [2] [3].

From a technology perspective, while MBSFN was developed in LTE and uses Single Frequency Network (SFN), SFN itself was not new and had been investigated decades ago for classical broadcast technologies, such as Digital Audio Broadcasting (DAB) and Digital Video Broadcasting (DVB) [4] [5]. These early works demonstrated that SFN could improve coverage and spectrum usage.

While both LTE MBSFN and classical broadcasting technologies use SFN, LTE MBSFN operates under LTE architecture and follows LTE protocol stacks. System performance is hence different, which triggered studies of LTE MBSFN in recent years from various perspectives. In [6], the authors first derived an analytical expression for SINR at a given point in a cell, then evaluated MBSFN performance under different Modulation and Coding Schemes (MCSs), the length of cyclic prefix, and the impact of shadowing. In [7], the authors extended the work in [6] to femtocell and compared single cell transmissions with multicell transmissions. None of the above work considered multiple antennas at the transmitter side or the receiver side. These multiple antennas allow multiple-input and multiple-output (MIMO) in unicast, which is one major technology that made LTE successful. In addition, the performance between MBSFN and unicast are compared in [8], where the authors used average MCS for all user equipments (UEs) for performance calculation. In [9], the authors proposed an optimal UE grouping algorithm in MBSFN, where the UEs were associated with the same MCS in unicast and multicast transmissions. As shown in our previous work [10], this is not always the case. MCSs could be different for different UEs, and MCSs used for unicast and multicast could be different for the same UE as well.

In this paper we investigate LTE MBSFN from the perspectives of throughput, resource efficiency, MBSFN gain, and outage. Unlike commercial broadcasting in a large deployment area, public safety incidents could vary in size and happen within a small area. Therefore we also consider small MBSFN areas. Specifically, we first derive an SINR analytical model for MBSFN. Different from others' work, multiple antennas, multipath channel, and equalizer are considered. The resulting model is hence more realistic and accurate. Next, by closely following the 3rd Generation Partnership Project (3GPP) standards, we implement the MBSFN SINR model and develop an MBSFN system level simulator as well as a simulation platform to compare unicast and MBSFN performance. Different from others' work, here SINR values in unicast and MBSFN are calculated separately based on their unique models. The high fidelity MBSFN Block Error Rate (BLER) curves and Channel Quality Indicator (CQI) switch points from our previous work [10] are also employed for PHY abstraction. Then, through comprehensive simulations, we show that although unicast may have higher resource efficiency in terms of information bits/symbol, MBSFN would provide higher throughput since it uses the full bandwidth in each transmission that serves all first responders, while in unicast resources are shared among first responders. Simulation

results also confirmed that larger MBSFN area size would increase MBSFN throughput due to higher MBSFN diversity combining gain and less interference. We further quantify MBSFN SINR improvement from diversity combining and interference reduction, respectively. The results show that while at cell edge they are comparable, at cell center the gain from interference reduction dominates and is significantly higher. However, the large SINR gain at cell center would not improve performance significantly due to MCS cap and lack of MIMO support for MBSFN. Finally, simulation results show that compared with unicast, MBSFN improves outage probability significantly, which is essential for public safety incidents. The above MBSFN performance improvements hold even when the MBSFN area size is one cell, which applies to the case when the public safety incident area is small.

The rest of the paper is organized as follows. In Section II we briefly describe unicast and MBSFN details as specified in 3GPP that are relevant to our analysis. In Section III we derive the SINR analytical model for MBSFN. In Section IV we describe our simulation design, together with simulation results and analysis. In Section V we summarizes our findings.

II. Review of Unicast and MBSFN in LTE

In this section we review unicast and MBSFN as specified by 3GPP, with emphasis on factors that have direct impacts on our analysis. The public safety broadband network Band 14 (B14) 10 MHz bandwidth Frequency Division Duplexing (FDD) is used as an example [11], with a focus on downlink.

A. LTE Overview

3GPP specifies Orthogonal Frequency-Division Multiple Access (OFDMA) for LTE downlink, and Cyclic Prefix (CP) is used to avoid Inter-Symbol Interference (ISI) [12]. Both normal CP and extended CP are specified. While the normal CP is used in typical LTE deployments to achieve high data rate, the extended CP is used in special cases such as in very large cells and MBSFN. In this paper, normal CP is used in unicast analysis, and extended CP is used for MBSFN.

For FDD, 3GPP defines frame structure type 1 [13], where one radio frame is 10 ms in duration and divided into 10 subframes. The smallest time-frequency unit for downlink transmission is a resource element (RE), which consists of one Orthogonal Frequency Division Multiplex (OFDM) subcarrier for a duration of one OFDM symbol. Transmissions can be scheduled by Resource Blocks (RBs) [14], and data is carried in Transport Blocks (TBs), which are passed from the Media Access Control (MAC) layer to the PHY layer once per Transmission Time Interval (TTI) which is 1 ms.

UEs report channel quality back to eNodeB using different sets of CQI indices for different MCS sets the network may deploy. In this paper, we consider the MCS set of Quadrature Phase Shift Keying (QPSK), 16 Quadrature Amplitude Modulation (QAM), and 64QAM. The corresponding CQI indices and their interpretations are given in Table 7.2.3-1 in [13].

B. LTE Unicast Review

For unicast, RB is the basic unit when allocating resources. To improve data rate and robustness, LTE unicast utilizes MIMO technology such as transmit diversity, spatial multiplexing, and beamforming. Accordingly, 3GPP defines 10 transmission modes (TMs) and could support up to 8 layer transmissions using TM9 [14], which is the transmission mode used in this paper. In addition, since Hybrid Automatic Repeat Request (HARQ) is specified for unicast transmissions, in this paper the target BLER is selected to be 10 %.

C. LTE MBSFN Review

In MBSFN, data is transmitted from multiple cells to the destination UE, as shown in Figure 1. All cells involved are tightly synchronized and transmit the same content over the same subcarriers using the same waveform. These cells form a so-called MBSFN area. To avoid ISI, the transmissions from different cells are targeted to arrive at the UE within CP at the start of the symbol. Hence 3GPP specifies the extended CP for MBSFN. From the UE perspective, the UE could treat all the transmissions from MBSFN area in the same way as multipath components of a single cell transmission, and the SINR could improve especially at cell edge. Note that the SINR improvement comes from two folds. One is the diversity combining gain from multiple signal sources. Another is the reduction of inter-cell interference - the transmissions from additional MBSFN cells are now turned into constructive signals instead of inter-cell interference. In Section IV-C, we will quantify the SINR improvement from these two folds.

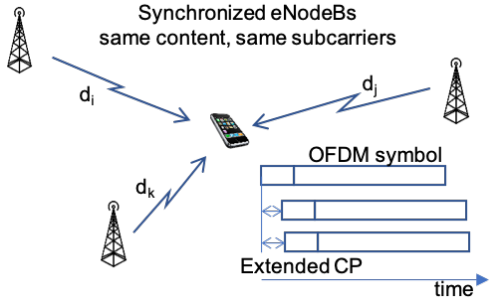

Fig. 1. MBSFN Transmission [15]

The composite channel from multiple cells in MBSFN requires a separate channel estimation from that performed from a single cell. 3GPP hence defines MBSFN subframe that carries MBSFN reference signals. MBSFN data is transmitted in MBSFN subframes only while unicast data is transmitted in non-MBSFN subframes, and MBSFN subframes and non-MBSFN subframes are interleaved in time. In addition, out of the 10 subframes within one radio frame, subframe 0, 4, 5, and 9 carry control information that is essential for network operation, such as paging occasions [14]. These four subframes are hence reserved for unicast transmissions and cannot be configured as MBSFN subframes. Therefore, there are at most six subframes available for MBSFN transmissions, or 60 % of the total resources.

3GPP also specifies that a single TB is generated per TTI for multicast channel (MCH) and uses all the MBSFN resources in that subframe [16] (e.g. 50 RBs for public safety band B14). In addition, no transmit diversity scheme is specified, and MCH is mapped on a single layer spatial multiplexing. Hence MBSFN could not take advantage of MIMO technologies. Furthermore, given its multicast nature, 3GPP specifies no radio link control retransmissions and no HARQ for MBSFN. Hence, in order to deliver acceptable service to upper layers, lower target BLER is typically used for MBSFN. In this paper we use 1 %.

III. MBSFN Analytical Model

In this section we derive an analytical model for MBSFN SINR, considering multiple antennas, multipath channel, and equalizer. We then convert it into Additive White Gaussian Noise (AWGN) equivalent SINR, which will later be fed into system level simulations.

A. MBSFN Networks

Consider a regular hexagonal network with three sectors per cell, as illustrated in Figure 2, where the numbers are cell identifiers (IDs). Let $\mathcal{I}$ denote the set of cells under consideration, and N denote the total number of cells in set $\mathcal{I}$. Index these N cells such that the first N_{M} cells are cells that participate in MBSFN transmissions within the MBSFN area (cell 1 to 21 in Figure 2), and denote them by set $\mathcal{I}_{\text{M}} = \{1, 2, \cdots, N_{\text{M}}\}$. Consequently, the cells with indices among $N_{\text{M}}+1, \cdots, N$ are the cells that do not participate in MBSFN transmissions (the cells that are not assigned an ID in Figure 2). Denote them by set $\mathcal{I}_{\text{L}} = \{N_{\text{M}}+1, N_{\text{M}}+2, \cdots, N\}$, where its size $N_{\text{L}} = N - N_{\text{M}}$. All cells have the same number of transmit antennas N_{Tx}, and all UEs have the same number of receiver antennas N_{Rx}.

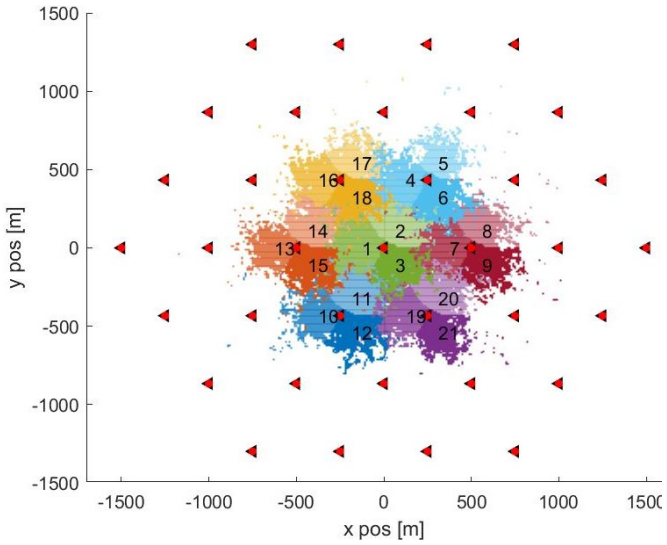

Fig. 2. Network Layout with Cell ID

Consider a UE within the MBSFN area. As shown in Figure 1, let d_i denote the distance between MBSFN cell $i \in \mathcal{I}_{\text{M}}$ and the UE, while MBSFN cell $k \in \mathcal{I}_{\text{M}}$ be the cell that is closest to the UE. As mentioned previously, in MBSFN, all MBSFN cells are tightly synchronized and transmit the same content simultaneously at the same subcarriers. Use the first signal received from cell k as the reference signal, and align to it all signals received after, including those from other MBSFN cells. Then the signals from cell i incur delay τ_i [6] [4]:

$$\tau_i = \frac{d_i - d_k}{s}, \tag{1}$$

where s is the speed of light. Note that given the relatively long CP length and signal frame - 16.67 μs for the extended CP length and 66.67 μs for the signal frame per 3GPP - the delays from different paths from the same cell i are not further differentiated, and are all approximated by the same τ_i.

The constructive and destructive portions of the signal from cell i, $i \neq k$ ($i \in \mathcal{I}_{\text{M}}$) can be captured by weight function ω_i and $1 - \omega_i$, respectively, where ω_i is as below [6] [4]:

$$\omega_i = \begin{cases} 1 & \text{when } 0 \leq \tau_i < T_{\text{CP}} \\ 1 - \dfrac{\tau_i - T_{\text{CP}}}{T_{\text{u}}} & \text{when } T_{\text{CP}} \leq \tau_i < T_{\text{CP}} + T_{\text{u}} \\ 0 & \text{otherwise} \end{cases} \tag{2}$$

where T_{CP} is the extended CP length defined in 3GPP for MBSFN, and T_{u} is the length of the useful signal frame.

Note that the destructive portion leads to ISI for the next symbol.

B. RE Level SINR

As mentioned in Section II, 3GPP specifies that a single TB per TTI is used for MBSFN transmission, and this TB uses all resources in that subframe. Let N_{RE} denote the total number of REs within one MBSFN subframe, and index the REs by $c = 1, 2, \cdots, N_{\text{RE}}$. Then the $(N_{\text{Rx}} \times 1)$-element UE received signal vector at RE c, denoted by $\boldsymbol{y}^c$, can be expressed as

$$\begin{aligned} \boldsymbol{y}^c = & \sum_{i=\mathcal{I}_{\text{M}}} \sqrt{\omega_i P_i^c} \boldsymbol{H}^{(i,c)} \mathbf{1}_{N_{\text{Tx}}} x_m \\ & + \sum_{i=\mathcal{I}_{\text{M}}} \sqrt{(1-\omega_i) P_i^c} \boldsymbol{H}^{(i,c)} \mathbf{1}_{N_{\text{Tx}}} x_m^- \\ & + \sum_{l=\mathcal{I}_{\text{L}}} \sqrt{P_l^c} \boldsymbol{H}^{(l,c)} \boldsymbol{W}^{(l,c)} \boldsymbol{\chi}_l + \boldsymbol{n}^c, \end{aligned} \tag{3}$$

where x_m is the MBSFN transmit signal, x_m^- is the previous MBSFN transmit signal; $\boldsymbol{\chi}_l$ is the $(N_{\text{Tx}} \times 1)$-element transmit signal vector from cell l, $l \in \mathcal{I}_{\text{L}}$ (i.e. $l \notin \mathcal{I}_{\text{M}}$); P_i^c and P_l^c ($i \in \mathcal{I}_{\text{M}}$, $l \in \mathcal{I}_{\text{L}}$) are the signal powers from cell i and l at RE c after taking into account path loss and shadowing but without small-scale fading, respectively; $\boldsymbol{H}^{(i,c)}$ and $\boldsymbol{H}^{(l,c)}$, ($i \in \mathcal{I}_{\text{M}}$, $l \in \mathcal{I}_{\text{L}}$) are the $(N_{\text{Rx}} \times N_{\text{Tx}})$-element matrices representing the frequency domain channel gains from cell i and l to the UE at RE c, respectively; $\boldsymbol{W}^{(l,c)}$ is the $(N_{\text{Tx}} \times N_{\text{Tx}})$ channel precoding matrix used by cell l on RE c, $l \in \mathcal{I}_L$; $\mathbf{1}_{N_{\text{Tx}}}$ is $(N_{\text{Tx}} \times 1)$ column vector with all elements being 1; and $\boldsymbol{n}^c$ represents thermal noise with zero mean and variance σ_N^2.

The first term in Eq. (3) represents the constructive portion of the signal. The second term represents the ISI from the

destructive portion of the previous transmit signal, where the channel experienced by this destructive portion is approximated by the channel experienced by the current signal. The third term represents interference from the non-MBSFN cells. And the last term represents the thermal noise. Note that all MBSFN cells and all transmit antennas at each MBSFN cell transmit the same signal. Hence x_m applies to all MBSFN cell $i = 1, \cdots, N_{\mathrm{M}}$ and each of their transmit antennas. x_m is hence essentially a scalar.

Define

$$\boldsymbol{q}^c = \left[\sqrt{\omega_1 P_1^c}\boldsymbol{H}^{(1,c)}, \cdots, \sqrt{w_{N_{\mathrm{M}}} P_{N_{\mathrm{M}}}^c}\boldsymbol{H}^{(N_{\mathrm{M}},c)}\right] \mathbf{1}_{(N_{\mathrm{Tx}})(N_{\mathrm{M}})}, \tag{4}$$

where $\mathbf{1}_{(N_{\mathrm{Tx}})(N_{\mathrm{M}})}$ is $(N_{\mathrm{Tx}} \cdot N_{\mathrm{M}} \times 1)$-element column vector with all elements being 1. Then:

$$\boldsymbol{y}^c = \boldsymbol{q}^c x_m + \sum_{i=1}^{N_{\mathrm{M}}} \sqrt{(1-\omega_i)P_i^c}\boldsymbol{H}^{(i,c)}\mathbf{1}_{N_{\mathrm{Tx}}} x_m^- + \sum_{l=N_{\mathrm{M}}+1}^{N} \sqrt{P_l^c}\boldsymbol{H}^{(l,c)}\boldsymbol{W}^{(l,c)}\boldsymbol{\chi}_l + \boldsymbol{n}^c. \tag{5}$$

Eq. (5) shows that the system could be viewed as a Single Input Multiple Output (SIMO) system, with signals from transmit antennas of all MBSFN cells being treated as the same transmit signal from different paths. We could hence apply zero-forcing receiver

$$\boldsymbol{f}^c = [(\boldsymbol{q}^c)^H \boldsymbol{q}^c]^{-1}(\boldsymbol{q}^c)^H, \tag{6}$$

where the superscript $(\cdot)^H$ represents conjugate transpose. Then the post-equalization received signal becomes

$$r^c = \boldsymbol{f}^c \boldsymbol{y}^c \tag{7}$$

$$= x_m + \sum_{i=1}^{N_{\mathrm{M}}} \sqrt{(1-\omega_i)P_i^c}\boldsymbol{f}^c\boldsymbol{H}^{(i,c)}\mathbf{1}_{N_{\mathrm{Tx}}} x_m^- + \sum_{l=N_{\mathrm{M}}+1}^{N} \sqrt{P_l^c}\boldsymbol{f}^c\boldsymbol{H}^{(l,c)}\boldsymbol{W}^{(l,c)}\boldsymbol{\chi}_l + \boldsymbol{f}^c\boldsymbol{n}^c. \tag{8}$$

The post-equalization SINR for RE c can then be calculated as below:

$$\gamma^c = \left(\sum_{i=1}^{N_{\mathrm{M}}} (1-\omega_i) P_i^c \|\boldsymbol{f}^c \boldsymbol{H}^{(i,c)} \mathbf{1}_{N_{\mathrm{Tx}}}\|^2 + \sum_{l=N_M+1}^{N} P_l^c \|\boldsymbol{f}^c \boldsymbol{H}^{(l,c)} \boldsymbol{W}^{(l,c)}\|^2 + \|\boldsymbol{f}^c\|^2 \sigma_N^2 \right)^{-1} \tag{9}$$

C. AWGN Equivalent SINR

In our analysis, Mutual Information Effective SINR Mapping (MIESM) based PHY abstraction is employed to link system level simulation and link level simulation [17]. Let $f_m(\cdot)$ be the Bit-Interleaved Coded Modulation (BICM) capacity of modulation alphabet m that is associated with the MCS m. Then, across all N_{RE} REs used for the MBSFN TB transmission, the equivalent SINR over AWGN channel for modulation m is:

$$\gamma_m = f_m^{-1}\left[\frac{1}{N_{\mathrm{RE}}}\sum_{c=1}^{N_{\mathrm{RE}}} f_m(\gamma^c)\right]. \tag{10}$$

This AWGN equivalent TB SINR γ_m, together with the AWGN BLER curves, target BLER 1 %, and CQI switching points [10], is used for MCS selection and CQI reporting in system level simulations, as well as packet loss determination when the UE receives a packet.

IV. Simulation Design and Results

A. Simulation Design

The simulation flow chart is illustrated in Figure 3. For comparison purpose, there are two branches, one for unicast and one for MBSFN. Both are run for the same scenario settings. The unicast branch follows Vienna system level simulator [17][1], with TM9 selected. The MBSFN branch utilizes the analytical model derived in Section III. Due to the stringent requirement on transmission reliability in public safety incidents, the minimum MCS among first responders is selected for MBSFN transmissions.

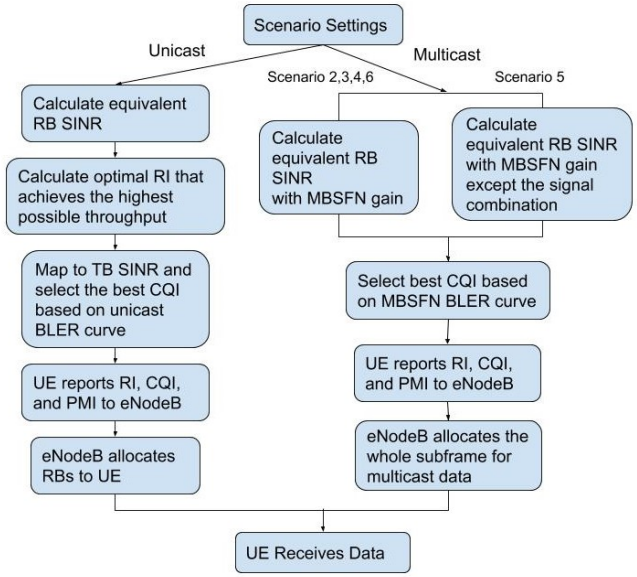

Fig. 3. Simulation Flowchart

The network simulated is a regular hexagonal network with three sectors per cell, as shown in Figure 2, where the numbers are cell IDs and outer rings are included to simulate interference. Public safety band B14 is selected and consider 8 x 4 MIMO configuration. Channel models used are the urban and rural models defined by 3GPP [18] for path loss, Claussen model for shadowing [19], and International Telecommunication Union (ITU) PedB, VehA, and VehB for small scale fading, with speed 10 km/h, 30 km/h, and 120 km/

[1]Any mention of commercial products in the paper is for information only; it does not imply recommendation or endorsement by National Institute of Standards and Technology.

h, respectively. Inter-site-distance (ISD) studied are 500 m, 1299 m, and 1732 m. Later we use urban ISD1299 VehA to denote urban path loss, ISD 1299 m, and VehA with speed 30 km/h. Other channel notations can be explained similarly. The number of runs and TTIs are chosen to capture statistically stable results.

Table I summarizes the six scenarios simulated for performance analysis, where scenario 5 is designed for MBSFN gain analysis used in Section IV-C and will be described there. The scenarios with different MBSFN area sizes are illustrated in Figure 4, where each color represents a tri-sector site and different color transparency shows different cells within a site. Note that scenarios 2 to 4 have small MBSFN areas to cover public safety incidents with small areas, and scenario 6 has a large enough MBSFN area to cover public safety incidents with large areas.

TABLE I
SIMULATION SCENARIOS

Scenario	Transmission
1	Unicast
2	MBSFN area: cell 1
3	MBSFN area: cell 1-2
4	MBSFN area: cell 1-3
5	MBSFN area: cell 1-21, No Signal Combination
6	MBSFN area: cell 1-21

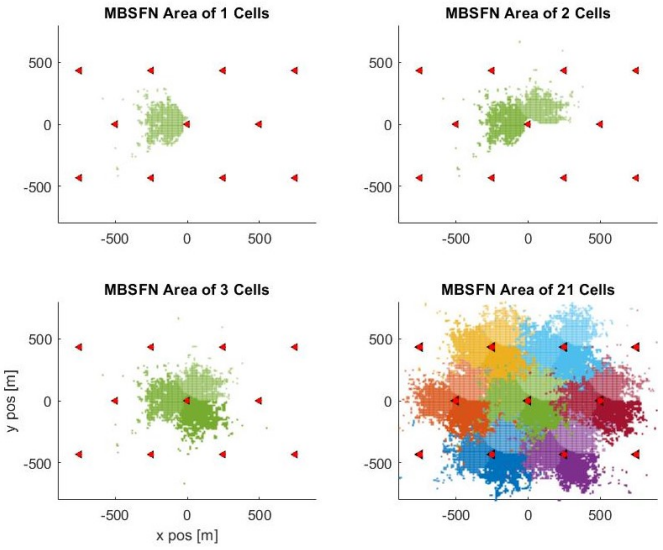

Fig. 4. MBSFN Deployment Scenarios

B. Resource Efficiency and Throughput

In this section we investigate resource efficiency for unicast and MBSFN as well as throughput experienced by first responders. For resource efficiency, the metric studied is information bits/symbol as in Table 7.2.3-1 in [13]. For unicast, in case there is more than one layer from spatial multiplexing, there are two codewords. Information bits/symbol is then the sum of bits/symbol from both codewords.

Scenario 1, 2, 3, 4, and 6 in Table I are simulated for this study, and 10 UEs are dropped uniformly within cell 1. Urban ISD1299 VehA channel is employed, proportional fairness is applied for scheduler, and 50 runs are performed. The resulting cumulative distribution function (CDF) of UE information bits/symbol is shown in Figure 5, where each UE contributes one sample. UE bits/symbol is calculated as the average bits/symbol over total resource units. Specifically, for unicast, it is averaged over all RBs and 300 TTIs. For MBSFN, it is averaged over all TTIs as a single TB is used per TTI (Section II).

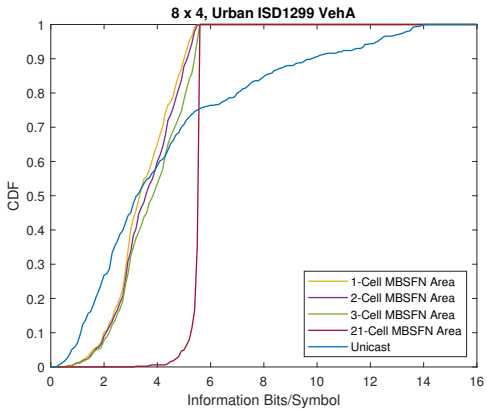

Fig. 5. Unicast vs MBSFN - Information Bits/Symbol

As expected, Figure 5 shows that larger MBSFN size leads to higher bits/symbol. This is because a larger MBSFN area implies more cells participating in MBSFN transmissions, hence the higher diversity combining gain, the less destructive interference, and the higher bits/symbol (Section III).

In addition, Figure 5 also shows that unicast has larger spread. The higher bits/symbol values come from multi-layer-transmissions due to spatial multiplexing in TM9 while the lower values are due to the lack of diversity combining gain.

Nevertheless, the possible higher bits/symbol of unicast does not necessarily imply higher throughput. The CDF of UE throughput from the same simulations is plotted in Figure 6.

Figure 6 shows that although unicast may have higher resource efficiency for individual UEs, MBSFN always has higher throughput. This holds even when the MBSFN area size is one cell. The reason is that in MBSFN each transmission serves all UEs and utilizes all RBs, whereas in unicast each transmission serves one UE and could use only a fraction of all RBs (10 UEs share the total RBs in each run). The more UEs being served, the less RBs each UE gets, and the less resulting throughput. Note that as mentioned in Section II, only 60 % of subframes are used in MBSFN. That is, MBSFN achieves higher throughput with only 60 % of the resources.

Figure 6 also shows that a larger MBSFN area leads to higher throughput. As with the previous analysis, this is because a larger MBSFN area leads to higher diversity combining gain and less destructive interference, and hence higher throughput.

Similar simulations were run for additional channels, and Table II lists the differences in median throughput between MBSFN and unicast, with unicast median throughput as the

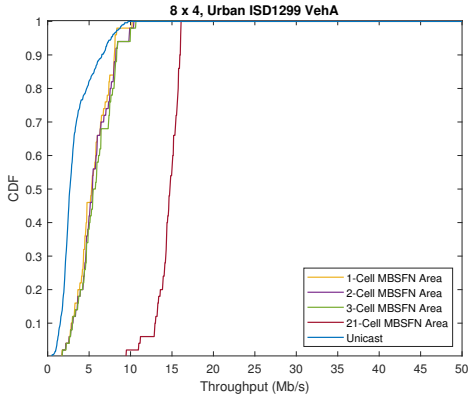

Fig. 6. Unicast vs MBSFN - Throughput

reference point. It can be seen that the trend of higher throughput with larger MBSFN size holds for all channels, and the median throughput delta between unicast and MBSFN can exceed 3 Mb/s.

TABLE II
THROUGHPUT DELTA BETWEEN UNICAST AND MBSFN (MB/S)

MBSFN area size	1 cell	2 cells	3 cells	21 cells
Rural ISD1299 VehB	0.5	0.6	0.6	3.1
Rural ISD1732 VehB	0.6	0.8	1.0	2.8
Urban ISD500 PedB	0.5	0.8	0.9	2.0
Urban ISD500 VehA	0.6	0.8	1.0	2.1
Urban ISD1299 VehA	0.1	0.3	0.6	2.3
Urban ISD1299 VehB	0.1	0.4	0.7	2.3

C. Sources of MBSFN Gain

As mentioned in Section II, the performance enhancement of MBSFN mainly comes from two sources: the diversity combining gain from multiple signal sources (cells), and the reduction of inter-cell interference. In this subsection we quantify the contribution of these two sources to MBSFN TB SINR incurred by a random UE (Equation 10). Note that the TB SINR for a UE directly reflects the physical channel experienced by the UE and is used for MCS selection. Hence it reflects the upper bound of the achievable throughput for the UE, and impacts its actual throughput as well.

For this purpose, the test scenario 5 is designed. In its SINR calculations and except for cell 1, power from other MBSFN cells is not included into neither the signal portion nor the interference portion. Hence, compared with scenario 2, inter-cell interference is removed. And compared with scenario 6, there is no diversity combining gain.

All these three scenarios - scenario 2, 5, and 6 - are simulated for 1000 TTIs, and UEs are dropped to cover the entire cell 1 (refer to Figure 4). Figure 7 plots the sorted MBSFN TB SINR in scenario 2, together with MBSFN gains from interference reduction, diversity combining, and the sum of both, respectively. Since the data is sorted by TB SINR, low UE index range maps to cell edge, and high UE index range maps to cell center. It can be seen that from cell edge to cell center, while the diversity combining gain decreases, the gain from interference reduction increases significantly. This is because the power from other MBSFN cells decreases when going from cell edge to cell center. Whereas at cell edge the two gains are comparable, around 5 dB, at cell center the gain from interference reduction dominates and the overall gain could be as high as around 20 dB. Unfortunately, this big SINR improvement at cell center would not lead to significant performance improvement due to the cap of the highest MCS (refer to Table I in [10]) and lack of MIMO technologies (Section II). Note that from the CQI switching points in the table, the maximum CQI 15 can be achieved when SINR is 20.5 dB or above, which can be achieved at cell center without the SINR improvement (the TB SINR in scenario 2). Figure 8 shows MBSFN TB SINR with UE locations, which further verifies the above analysis.

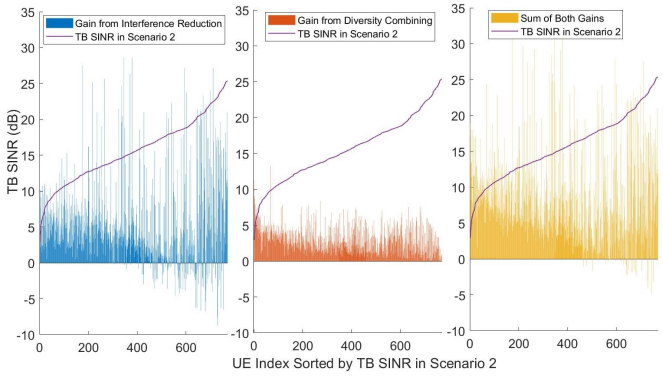

Fig. 7. Sources of MBSFN Gain

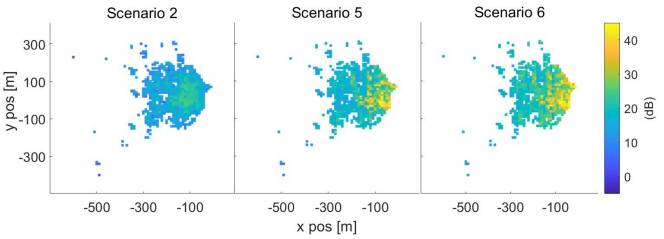

Fig. 8. TB SINR with UE Position

D. Outage Probability

In this subsection we quantify improvements in outage probability generated by using MBSFN. Consider a UE dropped randomly at a cell at a random time and being allocated a random resource chunk. In unicast, the resource chunk considered is five RBs, while in MBSFN it is one subframe. The outage probability considered in this paper is defined as the probability that the information bits/symbol of this UE is below a threshold.

To capture this outage probability, for each scenario listed in Table I except scenario 5, UEs are dropped to cover the entire cell 1, and simulations are run for 2000 TTIs. The resulting outage probability as a function of the threshold is plotted in Figure 9. The figure shows a significant decrease in outage probability when using MBSFN for all MBSFN sizes studied. As with the previous analysis, this is because of diversity combining and interference reduction in MBSFN. The larger

the MBSFN area size, the smaller the outage probability is. For example, when the threshold is 1 bit/symbol, the outage probability for unicast is around 4.5 %, while for MBSFN it is less than 0.2 % for MBSFN area sizes of 1 to 3 cells, and 0 % for 21 cells. Note that the significant decrease in outage probability holds even for an MBSFN area size of one cell.

Table III shows the achievable information bits/symbol when the outage probability is 2 % and 5 %, respectively. With the same planned outage probability, the table also shows a significant increase in achievable bits/symbol from unicast to MBSFN. Due to quantization, the bits/symbol is the same with MBSFN area size of 1, 2, and 3 cells. While with area size of 21 cells, the achievable bits/symbol is significantly higher.

TABLE III
INFORMATION BIT/SYMBOL WITH OUTAGE PROBABILITY

Scenario	1	2	3	4	6
2 %	0.83	1.91	1.91	1.91	3.32
5 %	1.17	1.47	1.47	1.47	4.52

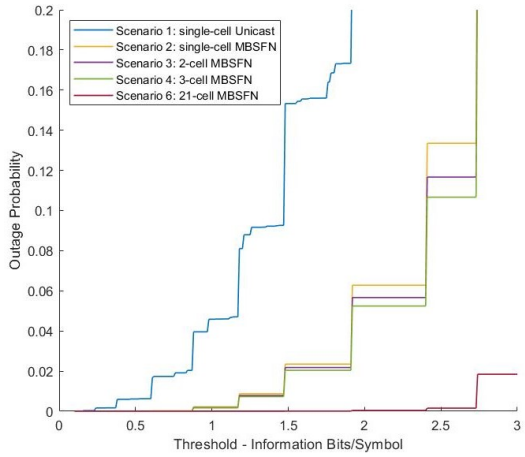

Fig. 9. Outage Probability with Threshold

V. CONCLUSION

To meet first responders' communication requirements, in this paper LTE MBSFN and unicast were investigated from the perspectives of throughput, information bits/symbol, sources of MBSFN gain, and outage probability. First, we derived an accurate MBSFN SINR analytical model. Then, through comprehensive MBSFN and unicast simulations, we showed that although the physical channels in unicast may be more efficient with higher information bits/symbol, MBSFN would provide higher throughput since the resources are not shared among UEs as in unicast. We also validated that a larger MBSFN area size would increase the MBSFN throughput due to higher MBSFN diversity combining gain and less interference. We further demonstrated that SINR improvement due to MBSFN diversity combining gains and interference reduction are comparable at cell edge, while the high MBSFN SINR improvement at cell center does not lead to significant performance improvement due to MCS cap and lack of MIMO support for MBSFN. Finally, compared with unicast, MBSFN improves outage probability significantly, which is essential for public safety incidents. All the above results hold not only for large MBSFN area sizes as in commercial networks, but also for small MBSFN area sizes, which cover cases where the incident area is small.

Since resource sharing is one major factor that limits unicast performance, our next step is to investigate the impact of number of first responders on MBSFN performance improvement over unicast. In addition to throughput, we will introduce other performance metrics as well, such as flight time, and further investigate the trade-offs between unicast and MBSFN.

REFERENCES

[1] "Minnesota Department of Public Safety Public Safety Wireless Data Network Requirements Project Needs Assessment Report," Minnesota PSN, Tech. Rep., May, 2011.

[2] J. Song and R. Phung, "Emergency group call over embms," in *16th International Conference on Advanced Communication Technology*, Feb 2014, pp. 1017–1022.

[3] T. Doumi, M. F. Dolan, S. Tatesh, A. Casati, G. Tsirtsis, K. Anchan, and D. Flore, "Lte for public safety networks," *IEEE Communications Magazine*, vol. 51, no. 2, pp. 106–112, February 2013.

[4] R. Rebhan and J. Zander, "On the outage probability in single frequency networks for digital broadcasting," *IEEE Transactions on Broadcasting*, vol. 39, no. 4, pp. 395–401, Dec 1993.

[5] G. Malmgren, "On the performance of single frequency networks in correlated shadow fading," *IEEE Transactions on Broadcasting*, vol. 43, no. 2, pp. 155–165, June 1997.

[6] L. Rong, O. B. Haddada, and S. Elayoubi, "Analytical analysis of the coverage of a mbsfn ofdma network," in *IEEE GLOBECOM 2008 - 2008 IEEE Global Telecommunications Conference*, Nov 2008, pp. 1–5.

[7] F. X. A. Wibowo, A. A. P. Bangun, A. Kurniawan, and Hendrawan, "Multimedia Broadcast Multicast Service over Single Frequency Network (MBSFN) in LTE based Femtocell," in *Proceedings of the 2011 International Conference on Electrical Engineering and Informatics*, July 2011, pp. 1–5.

[8] S. Mitrofanov, A. Anisimov, and A. Turlikov, "eMBMS LTE Usage to Deliver Mobile Data," in *2014 6th International Congress on Ultra Modern Telecommunications and Control Systems and Workshops (ICUMT)*, Oct 2014, pp. 60–65.

[9] J. Chen, M. Chiang, J. Erman, G. Li, K. K. Ramakrishnan, and R. K. Sinha, "Fair and Optimal Resource Allocation for LTE Multicast (eMBMS): Group Partitioning and Dynamics," in *2015 IEEE INFOCOM*, April 2015, pp. 1266–1274.

[10] C. Liu, C. Shen, J. Chuang, A. R. Rouil, and H. Choi, "Throughput Analysis between Unicast and MBSFN from Link Level to System Level," in *IEEE 90th Vehicular Technology Conference*, September 2019.

[11] FirstNet. https://firstnet.gov/content/firstnet-building-nationwide-public-safety-network.

[12] J. Zhang, L. Yang, L. Hanzo, and H. Gharavi, "Advances in Cooperative Single-Carrier FDMA Communications: Beyond LTE-Advanced," *IEEE Communications Surveys Tutorials*, vol. 17, no. 2, pp. 730–756, Second quarter 2015.

[13] 3GPP TS36.213, "Evolved Universal Terrestrial Radio Access (E-UTRA); Physical Layer Procedures," 3GPP, Standard, Jan. 2019.

[14] 3GPP TS36.211, "Evolved Universal Terrestrial Radio Access (E-UTRA); Physical channels and modulation," 3GPP, Standard, Dec. 2018.

[15] S. Sesia, I. Toufik, and M. Baker, *LTE - The UMTS Long Term Evolution: From Theory to Practice: Second Edition*, August 2011.

[16] 3GPP TS36.300, "Evolved Universal Terrestrial Radio Access (E-UTRA) and Evolved Universal Terrestrial Radio Access Network (E-UTRAN); Overall description; Stage 2," 3GPP, Standard.

[17] M. Rupp, S. Schwarz, and M. Taranetz, *The Vienna LTE-Advanced Simulators: Up and Downlink, Link and System Level Simulation*, 1st ed. Springer Publishing Company, Incorporated, 2016.

[18] 3GPP TS36.942, "Evolved Universal Terrestrial Radio Access (E-UTRA); Radio Frequency (RF) system scenarios," 3GPP, , Jul. 2018.

[19] Claussen, "Efficient modelling of channel maps with correlated shadow fading in mobile radio systems," in *2005 IEEE 16th International Symposium on Personal, Indoor and Mobile Radio Communications*, vol. 1, Sep. 2005, pp. 512–516.